Development of spectrally self-switchable cover with phase change material for dynamic radiative cooling

Weiguang Su[1,2] [a], Ruigeng Kang[1,2], Pei Cai[1,2], Mingke Hu[3], Georgios Kokogiannakis[4], Jo Darkwa[3], Jun Chen[1,2], Shuhui Xu[1,2], Li Wang[1,2] [b]

1. School of Mechanical Engineering, Qilu University of Technology (Shandong Academy of Sciences), 250353, Jinan, China
2. Shandong Institute of Mechanical Design and Research, 250031, Jinan, China
3. Faculty of Engineering, University of Nottingham. University Park, Nottingham, NG7 2RD, UK.
4. Sustainable Buildings Research Centre, University of Wollongong, Australia

Abstract

Radiative cooling promises an effective strategy against global warming by sending waste heat to the deep universe in a passive manner. However, the mismatch between cooling supply and demand can significantly compromise the efficacy of spectrally-static radiative cooling devices in cold weather. Therefore, the present work introduced paraffin wax as the phase change material (PCM) to develop a spectrally self-switchable cover (SSC) for flexible radiative cooling. The transmittance of the paraffin wax at different temperatures, thicknesses and phases was characterized. In the UV-VIS-NIR band, the transmittance of the paraffin wax was over 90% in the liquid phase but below 5% in the solid phase. In the "atmospheric window" band, the transmission of the paraffin wax in the liquid phase was also much higher than that in the solid phase with a maximum difference of 41.1%. The optical constants of various paraffin waxes in solid and liquid phases were calculated according to the two-thickness inversion method. The average error of transmittance between the calculated and measured values was only 1.8% and 4% for the 0.19-1.1 μm and 8-13 μm bands, respectively. Moreover, the microstructure analysis of the solid-state paraffin wax revealed that the size of paraffin grains was around 10 μm with interlocking and irregular grain boundaries. The

[a] Corresponding author. E-mail address: wgsuper@hotmail.com; [b] Corresponding author. E-mail address: liwang@qlu.edu.cn.

integrated multilayered-like structure resulted in a significant transmittance reduction of the solid-state paraffin wax. In the end, self-switchable PE-PCM-PE (polyethylene-phase change material-polyethylene) covers were prepared and spectrally characterized. The paraffin-based cover provided a new and low-cost candidate solution for achieving dynamic radiative cooling.

Keywords: paraffin, phase change material, temperature adaptive, self-switchable cover, radiative cooling

Abbreviations:

AT	Average transmittance
DSC	Differential scanning calorimetry
FTIR	Fourier-transform infrared spectroscopy
MIR	Mid-infrared
NIR	Near-infrared
PCM	Phase change material
PCMs	Phase change materials
PE	polyethylene
PEA	polyethylene aerogel
SSC	Spectrally self-switchable cover
UV	Ultraviolet
vdW	van der Waals
VIS	Visible spectrum
VO_2	vanadium dioxide

Nomenclature:

Simple symbols	
A	Area of radiative cooler, m^2
k	Extinction coefficient of PCM in liquid, -
k_{solid}	Extinction coefficient of PCM in solid, -
L	Pathlength of the PCM, μm
L_1	Pathlength of the PCM sample-1, μm
L_2	Pathlength of the PCM sample-2, μm
n	Refractive index, %
t_{amb}	Ambient temperature,℃
t_{pcm}	Phase change temperature,℃
Greek symbols	

α	Absorptivity,%
ε	emissivity,%
ε_r	Radiative cooler emissivity,%
τ	Spectral transmittance, %
τ_{L1}	Spectral transmittance of the PCM sample-1,%
τ_{L2}	Spectral transmittance of the PCM sample-2,%
τ'	τ derivation of L,-
τ'_{liquid}	τ_{liquid} derivation of L,-
τ'_{solid}	τ_{solid} derivation of L,-
λ	Wavelength, μm
ρ	Spectral reflectance, %
ρ_{solid}	Spectral reflectance of solid sample, %

1 Introduction

Radiative cooling is a research hotspot for cooling and energy saving in buildings, which is achieved by radiative heat transfer between earth and outer space through the atmospheric window without consuming any extra energy [1]. An important development of a daytime radiative cooling device consisting of reflectors and thermal emitters was published in 2014 [2]. The efficiency of daytime radiative cooling mainly depends on the reflection coefficient of sunlight by reflectors and the emissivity of thermal emitters in the atmospheric window (8-13 μm). For instance, Raman et al. [2] fabricated a photonic radiative cooler consisting of seven layers of HfO_2 and SiO_2 radiator structure and a silver-coated reflector. The radiative cooler could reflect 97% of the incident sunlight and achieve a cooling power of 40.1 W/m^2 at a temperature of 4.9 ºC below ambient air temperature when exposed to a sunlight intensity power exceeding 850 W/m^2. Kou et al. [3] fabricated a three-layer radiator cooler consisting of 100 μm PDMS, 500 μm silica and 120 nm silver from top to bottom. The experimental results showed a cooling power of 127 W/m^2, and its surface temperature dropped 8.2 ºC below ambient temperature during the daytime. Chae et al. [4] proposed a daytime radiative cooler with a simple multilayer structure of inorganic materials of Al_2O_3, Si_3N_4, and SiO_2, and then optimized the stacking sequence and thickness of each layer by a particle swarm optimization method. The experimental test found that the

radiative cooler can reduce the temperature by up to 8.2 ºC under direct sunlight. Ma et al.[5] designed a seven-layered radiative cooler based on the differential evolutionary algorithm with a predicted cooling power of 87 W/m^2 and demonstrated an all-day cooling capability by experiment.

During experiments, a cover shield (convection barrier) with high transmission in the 8-13 μm on the top of the radiative cooler could separate the radiative cooler from the external environment [6], which can avoid dust accumulation, reduce the heat conduction and convection, improve the efficiency and service life of the radiative cooler. Tsilingris et al. [7] studied the infrared transmittance of various polymers, such as polymethyl methacrylate, glass fibre, polycarbonate, polyethylene, polypropylene, polyfluoroethylene, mylar film, polyimide and vinyl. The results concluded that polyethylene (PE) and polypropylene were suitable cover shield materials for radiation cooling systems due to high transmittance in the 8-13 μm spectrum band. In addition, Leroy et al. [8] developed a polyethylene aerogel (PEA) material as a cover shield over a conventional radiative cooler. Compared to the radiative cooler without the PEA cover, the cooling efficiency of the cooler with the PEA cover increased from 46 W/m^2 to 96 W/m^2 and the maximum cooling temperature increased from 3.8 ºC to 15 ºC under the solar radiation power of 936 W/m^2. However, static radiative coolers would increase the heating energy demand since the cooling cannot be automatically switched off in winter.

To automatically respond to the ambient temperature of radiative cooling systems, various self-adaptive radiative cooling systems were developed using phase change materials (PCMs) whose transmittance showed a significant change before and after the phase change [9]. For instance, vanadium dioxide (VO_2) [10] is at a transmissive insulating phase with a low emissivity in the infrared region when the temperature is below the phase change temperature of 68 ºC. On the contrary, VO_2 will switch to the metal state with a high emissivity when the temperature is above 68 ºC. Wang et al. [11] proposed the concept of a switchable infrared emitter based on VO_2 which can automatically switch on the radiative cooling when its structure temperature is below

68 ºC. Ono et al. [12] proposed a temperature self-adaptive radiative cooling system with eleven top layers of Ge/MgF_2 and three bottom layers of VO_2/MgF_2/W. Wu et al. [13] proposed a VO_2/SiO_2/VO_2 cavity structure, which can increase four times the radiative cooling power when the device temperature is higher than the phase change temperature of VO_2 (68 ºC). Long et al. [14] prepared a switchable absorber metamaterial with an aluminium sheet and a VO_2 film, which exhibited an absorption peak close to unity at the wavelength of 6.68 μm at room temperature. When the metamaterial was heated above the transition temperature of VO_2 (68 ºC), the absorption peak "switch-off". Abedini Dereshgi et al. [15] developed a tunable photonic device by combining VO_2 and van der Waals (vdW) materials that can also be used for regulating the temperature of a radiative cooling system. Zhao et al. [16] proposed a VO_2-based thermostat with the aid of tandem photonic crystals, whose average emissivity would increase from 0.06 to 0.95 when the VO_2 switched from insulator to the metal state. Xu et al. [17] successfully demonstrated a VO_2-based dynamic passive radiative cooling device in outdoor experiments. However, the fabrication of the above VO_2-based temperature adaptive radiative cooling systems required complex and expensive technologies [18], such as pulsed laser deposition [15], electron beam evaporation [14], direct-current magnetron sputtering and high-power impulse magnetron sputtering methods [17].

On the other hand, the paraffin wax as PCM also demonstrates transmittance switching properties in liquid and solid phases, and the price of paraffin wax (4.9 CNY/g [19]) is much cheaper than VO_2 (238.6 CNY/g [20]). Previous research by Zhao et al. [21] showed that the transmittance of paraffin wax (melting point at 32 ºC) in the liquid state is about 88% in the thickness of 1 mm and that value is much higher than the solid state of 3% in the thickness of 0.48 mm. Recently, Su et al. [22] prepared a series of temperature-responsive transmission switch film samples by integrating n-octadecane into polydimethylsiloxane as a form-stable PCM. To this end, paraffin wax demonstrates potential as low-cost switching material for radiative cooling. To overcome the leakage problem of melted paraffin and maintain the high transmittance

of the switching layer during a radiative cooling period, two high transmittance PE films in the 8-13um band [7] were proposed to seal a thin PCM layer and fabricate a simple three-layers structure of PE-PCM-PE film as a self-switchable cover (SSC). Meanwhile, the fabrication method of SSC is simple and much cheaper compared with VO_2.

To understand the transmittance and thermal response properties of the proposed low-cost SCC, the spectral transmittance of paraffin waxes at different temperatures, phases and thicknesses were initially studied. Then the optical constants (interfacial reflectance ρ and extinction coefficient k) of paraffin waxes were calculated by the two-thickness inversion method [23, 24] to resolve the transmittance switching principle of PCM. In the end, three types of triple-layer of PE-PCM-PE as a temperature adaptive spectrally self-switchable cover (SSC) were prepared, and their transmittance under switch-on and switch-off states were characterized.

2 Materials and methods

2.1 Materials

The aliphatic hydrocarbons have similar optical properties in the liquid phase due to the mimic molecular structure of C_nH_{2n+2}, and the melting point increases with their molecular mass [25]. To optimize the buildings' annual energy performance, the minimum switching-off temperature of radiative cooling should be no less than the lower limit of indoor temperature (16 ºC [26]) in buildings to avoid an over-cooling situation in winter, and the ideal phase change temperature should fit typical indoor thermal comfort temperature ranges (22 ºC to 28 ºC [27]). To investigate the optical switching properties of paraffin during phase change at different ambient temperatures, n-Hexadecane, n-Octadecane and n-Eicosane were selected as PCMs in this study, whose melting points in the range of 16.2 ºC to 35.0 ºC. Meanwhile, PE was chosen as encapsulation material to package and protect the PCM to produce SSC. Detailed

information on molecular composition, density, melting point and supplier of PCM and PE is shown in Table 1.

2.2 Preparation and characterization methods

2.2.1 Phase change properties of PCM

A differential scanning calorimetry (DSC) (TA25 Instruments Waters) equipment was used in determining the enthalpies of fusion and melting temperature of the n-Hexadecane, n-Octadecane and n-Eicosane samples. Before the measurement, the indicators of the DSC had been calibrated using temperature standard material. The PCM samples were tested following ISO 11357 Standards under the dynamic testing method in a nitrogen-protected environment at a cooling/heating rate of 1 ºC /min from 0 ºC to 50 ºC.

2.2.2 Spectral properties characterization of the PCM

An ultraviolet-visible spectrum (UV-VIS) spectrometer (UV-8000, Shanghai Metash Instruments Co., Ltd) was used to measure the spectral properties of n-alkanes in the band 0.19-1.1 μm with a spectral bandwidth of 1.8 nm. Before the measurement, the system baseline correction was performed, and the background of the air was removed based on a blank cuvette. The thickness of PCM samples was equal to the thickness of quartz cuvette at 1 mm, 2 mm and 3 mm. The PCM sample temperature was controlled by a semiconductor heating and cooling module (XH-W1504 Jiangsu Xinghe Electronic Technology Co., Ltd.) and circulating water. Meanwhile, a K-type thermocouple (TUT320D, UNI-Trend Technology (China) Co., Ltd) was used to monitor the PCM sample temperature. During the measurement of UV-8000, the temperature for three n-alkanes samples (Hexadecane, n-Octadecane and n-Eicosane) was kept at 50 ºC for the liquid phase and 5 ºC for the solid phase. The solidification process was used to analyze transmittance changes of PCM during the phase change period. The initial temperature of the samples was heated to 50 ºC and then cooled down

with 5 ºC circulating water. During the measurement of spectral transmittance, cooling water would be turned off to maintain a stable temperature of the PCM sample.

FTIR spectroscopy (BRUKER ALPHA, Germany) was used to measure the spectral transmittance of 2.5-25 μm for the three PCM samples. Before the measurement, the system baseline correction was performed, and the background of the air-KBr infrared absorption cell was removed. The PCM samples were filled within a KBr infrared absorption cell (HF-7 Tianjin Tianguang Optics Instrument Co., Ltd.), and the thickness was measured with an electronic spiral micrometer (0-25 μm, Dongguan Sanliang Precision Measuring Instrument Co., Ltd). During the measurements, the PCM was preheated to 70 ºC for the liquid phase and cooled to 0 ºC for the solid phase. At the same time, the K-type thermocouple was also used to measure the real-time temperature during the tests to confirm the phase of the PCM samples.

2.2.3 Preparation of SSC

Two layers of 100 μm PE film (2cm×2cm) were sealed by a heat sealer (BV106, Bonsen) forming three edges as a thin package, and then liquid PCM was injected into the PE package and sealed the final edge of the rectangular PE package. This resulted in an SSC composed of the three layers of PE-PCM-PE. The testing methods of SSC are the same as those of PCM, as described in 2.2.2 by UV-VIS and FTIR. Overall, the manufacture and testing equipment for PCM and SSC samples were summarized in Table. 2.

2.3 Two-thickness inversion method for PCM optical constants

The spectral transmission switching effects of paraffin are due to its optical constants changing during the phase change. To understand the relationship between the switching effect and optical constant changes, the two-thickness inversion method was therefore used to calculate the optical constants of paraffin in different phases. The two-thickness inversion method was developed by Tuntomo and Tien [24]. The relationship

between the transmittance (τ) at two thicknesses (L_1 and L_2) and the material characteristic parameters, i.e. interfacial reflectance (ρ), extinction coefficient (k) and refractive index (n) at the wavelength (λ) is as follows：

$$\tau_{L1} = \frac{(1-\rho)^2 \exp\left(\frac{-4\pi k L_1}{\lambda}\right)}{1-\rho^2 \exp\left(\frac{-8\pi k L_1}{\lambda}\right)} \quad (1)$$

$$\tau_{L2} = \frac{(1-\rho)^2 \exp\left(\frac{-4\pi k L_2}{\lambda}\right)}{1-\rho^2 \exp\left(\frac{-8\pi k L_2}{\lambda}\right)} \quad (2)$$

The interfacial reflectance (ρ) can be calculated by Fresnel law (3).

$$\rho = \frac{(n-1)^2+k^2}{(n+1)^2+k^2} \quad (3)$$

For liquid materials, the value of ρ is very small and ρ^2 tends to zero [23], so the $\rho^2 \exp\left(\frac{-8\pi k L_1}{\lambda}\right)$ can be neglected and Eqs. (1) and (2) simplified to:

$$\tau_{L1} = (1-\rho)^2 \exp\left(\frac{-4\pi k L_1}{\lambda}\right) \quad (4)$$

$$\tau_{L2} = (1-\rho)^2 \exp\left(\frac{-4\pi k L_2}{\lambda}\right) \quad (5)$$

T_{L1} and T_{L2} at the corresponding wavelength (λ) can be obtained from the UV-VIS-mid infrared (MIR) spectral test. According to L_1, L_2, T_{L1}, T_{L2} and λ and Eqs. (4) and (5), the k can be calculated by Eq. (6).

$$k = \frac{\lambda \ln\left(\frac{\tau_{L1}}{\tau_{L2}}\right)}{4\pi(L_1-L_2)} \quad (6)$$

Put Eq. (6) into Eq. (3) for a joint solution yields the results of the refractive index (n):

$$n = \frac{1+\rho+\sqrt{(1+\rho)^2-(1-\rho)^2(1+k^2)}}{1-\rho} \quad (7)$$

When the spectral reflectance (ρ) is unknown, it is not possible to use Eq. (7) to solve for the refractive index (n) of the liquid. Therefore, Eqs.4 and 5 are again combined to give the following result in Eq. (8).

$$\rho = 1 - \frac{\sqrt{\tau_{L1} \exp\left(\frac{-4\pi k L_1}{\lambda}\right)}+\sqrt{\tau_{L2} \exp\left(\frac{-4\pi k L_2}{\lambda}\right)}}{2} \quad (8)$$

However, for the solid material, the spectral reflectance (ρ) cannot be ignored. Therefore, the interfacial reflectance ρ and extinction coefficient k should be calculated by Eq. (9) and (10), respectively.

$$\rho_{solid} = \frac{1-\sqrt{{\tau_{L1}}^2+\tau_{L1}\left[\exp\left(\frac{4\pi k L_1}{\lambda}\right)-\exp\left(\frac{-4\pi k L_1}{\lambda}\right)\right]}}{1+\tau_{L1}\exp\left(-\frac{4\pi k L_1}{\lambda}\right)} \tag{9}$$

$$k_{solid} = \frac{\lambda \ln\left(1+\frac{\sqrt{1+4\left(\rho\frac{\tau_{L2}}{(1-\rho)^2}\right)^2}}{2\frac{\tau_{L2}}{(1-\rho)^2}}\right)}{4\pi L_2} \tag{10}$$

Matlab software (R2021a) was used for the iterative solution (see supplementary: M1_Formula-defining, M2_Calculation for liquid and M3_Calculation for solid). The calculation process of interfacial reflectance ρ and extinction coefficient k for PCM in liquid and solid phases are shown in Fig. 1.

The effect of the thickness L on the transmittance τ can be calculated by the change rate of transmittance (τ'), which is obtained by taking the derivative of Eq. (1) and Eq. (4). Therefore, the change rate of transmittance for solid (τ'_{solid}) and liquid (τ'_{liquid}) can be calculated in Eq. (11) and Eq. (12).

$$\tau'_{solid} = \frac{-(1-\rho)^2\frac{4\pi k}{\lambda}\left(e^{\frac{-4\pi k}{\lambda}}\right)^L-(1-\rho)^2\rho^2\frac{4\pi k}{\lambda}\left(e^{\frac{-4\pi k}{\lambda}}\right)^{3L}}{\left(1-\rho^2\left(e^{\frac{-4\pi k}{\lambda}}\right)^{2L}\right)^2} \tag{11}$$

$$\tau'_{liquid} = -(1-\rho)^2\frac{4\pi k}{\lambda}\left(e^{\frac{-4\pi k}{\lambda}}\right)^L \tag{12}$$

3 Results and discussion

3.1 Phase change temperature and latent heat

According to the DSC test results in Fig. 2 and Table 3, the solidification phase change temperature ranges for n-Hexadecane, n-Octadecane and n-Eicosane were 13.1 ºC ~ 14.4 ºC, 24.0 ºC ~ 25.3 ºC and 32.3 ºC ~ 34.6 ºC, respectively. At the same time, the

discharged latent enthalpies of 221.4 J/g, 243.3 J/g and 248.3 J/g were measured for the three samples. Different from n-Hexadecane and n-Octadecane, the solidification of n-Eicosane formed a metastable rotator phase and resulted in a sharp solid-solid transition that occurred between 32.3 ºC and 31.3 ºC when the rotator phase was transformed into a stable triclinic crystalline phase[28]. On the other hand, the melting phase change temperature ranges for n-Hexadecane, n-Octadecane and n-Eicosane were 16.2 ºC ~ 19.2 ºC, 26.1 ºC ~ 28.7 ºC and 35.0 ºC ~ 37.7 ºC, and the absorbed latent enthalpies of three PCMs were 220.5 J/g, 243.6 J/g and 248.0 J/g, respectively. The differences in latent heat for PCMs between melting and solidification were less than 1%, which indicated that the latent enthalpies were stable. Meanwhile, the subcooling temperature for n-Hexadecane, n-Octadecane and n-Eicosane were 1.8 ºC, 0.8 ºC and 0.4 ºC, respectively.

3.2 PCM transmittance measurements and analysis

3.2.1 Transmittance changes during the phase change process

As shown in Figs. 3 (a), (b) and (c), the spectral transmittance of the three PCM samples at a thickness of 1 mm was measured individually during the solidification process. Generally, the transmittance of PCM decreases from over 90% in the liquid phase to less than 5% in the solid phase. However, the decreasing rate of transmittance does not constitute a linear relationship with the solid-liquid ratio according to the temperature changes. For instance, the DSC curve in Fig. 2 shows a solidification temperature range between 13.1 ºC and 14.4 ºC for n-Hexadecane, but Fig. 3 (a) shows that the transmittance of n-Hexadcane abruptly dropped to 20% at 18.8 ºC. That means the measured solidification temperature by the K-type thermocouple was 4.4 ºC higher than the DSC value. The same phenomenon also appeared for n-Octadecane and n-Eicosane, and the freezing points were 3.1 ºC and 1.1 ºC higher than the DSC results, respectively. Furthermore, the transmittance for all three PCM samples was continuously decreased

even when the K-type thermocouple temperature remained constant. For example, the temperature of the n-Hexadcane sample was stabilized at 18.8 ºC for 20 minutes, and the sample transmittance decreased from 20% to 3% during that time. The n-Octadecane sample was held at 28.5 ºC for 3 minutes, and the transmittance decreased from 20% to 10%. The n-Eicosane sample was kept at 35.1 ºC for 2 minutes, and the transmittance decreased from 18% to 8%. These measurements show that the phase change of PCM samples did not stop after turning off the supply of cooling water. As a result, there was a continuous reduction of transmittance during the measurement.

The single transmittance measurement time (approximately 60 seconds) was much shorter than the PCM phase change time (over 20 minutes). However, it would not be appropriate to presume the PCM sample has no phase change during the measurement time even after turning off the supply of cooling water. This is because the phase change process of the PCM in the cuvette is not homogeneous but a gradual process from outside to inside. As shown in Figs. 3 (d), (e), (f) and (g), to avoid blocking the light path of UV-8000, the K-type thermocouple test point was not at the same position as the spectral measurement point. This misalignment also caused measurement errors during the correlation analysis between phase change temperature and transmittance. To this end, the solidification point of the three PCMs measured by K-type thermocouple was 1-3 ºC higher than the DSC results. Moreover, the temperature distribution in the cuvette was not uniform, as shown in Figs. 3 (f) and (g). This is due to the heating/cooling source being on the outside of the cuvette, and the heat transfer from outside to inside resulted in a temperature difference of 0-2 ºC. It was therefore concluded that the K-type thermocouple temperature was unable to represent the temperature of the whole PCM sample. For this reason, the following analysis will focus on the spectral transmission characteristics of paraffin in the solid and liquid phases.

3.2.2 Transmittance effect by phase and thickness in UV-VIS-NIR

The UV-VIS-NIR spectra transmittance (0.19-1.1 μm) of three PCM samples was

measured by UV-8000. The absorption peaks for the three PCMs were at 930 nm for n- Hexadecane, 928 nm for n-Octadecane and 926 nm for n-Eicosane, as shown in Figs. 4 (a), (c) and (e). However, the spectral transmittance is approximately the same for all n-Hexadecane, n-Octadecane and n-Eicosane samples, except at the absorption peaks.

The spectral transmittance curves of n-alkanes in the liquid phase with the thickness of 1mm, 2mm and 3mm are shown in Figs. 4 (a), (c) and (e). Generally, the transmittance of the liquid PCMs increased from UV to the VIS and stabilized at over 90%. For n-Hexadecane, the average transmittance (AT) in 0.4-1.1 μm decreased from 93.3% to 93.1% and to 92.8% when the thickness increased from 1 mm to 2 mm and to 3 mm, respectively. Similarly, for n-Octadecane, the average transmittance in 0.4-1.1 μm decreased from 93.6% to 93.1% and to 92.8% when the thickness increased from 1 mm to 2 mm and to 3 mm. For n-Eicosane, the average transmittance in 0.4-1.1 μm decreased from 93.1% to 92.3% and to 91.9% when the thickness increased from 1 mm to 2 mm and to 3 mm. The maximum reduction in transmittance was about 0.8% when the thickness of the PCM layer was doubled. Figs. 4 (b), (d), and (f) show the measured spectral transmittance of solid n-alkanes, which demonstrate a significant difference with the liquid state. In the solid phase cases, the PCM transmittance was below 5%, the peaks at the band around 350 nm from where onwards the transmittance gradually decreased to a constant value. In addition, the thickness appears to have a slightly negative effect on the transmission rate of solid n-alkanes. When the sample thickness was increased from 1 mm to 2 mm and to 3 mm, the average transmittance in the 0.4-1.1 μm band of n-Hexadecane decreased from 1.4% to 0.66% and to 0.64%, the average transmittance of n-Octadecane decreased from 1% to 0.7% and to 0.6%, the average transmittance of n-Eicosane decreased from 0.7% to 0.6% and to 0.6%. When doubling the PCM layer thickness in the solid phase, the maximum decrease in the average transmittance in the UV-VIS-NIR band was 0.7%. The above analysis in the 0.19-1.1 μm band shows that the PCMs have low spectral transmittance in the solid phase (below 5%) but a much higher spectral transmittance in the liquid phase (over 90%). Overall,

the effect of the phase change on the transmittance in the UV-VIS-NIR spectral band was much more significant than that of the thickness.

According to Eqs. (1) and (4), the transmittance of PCMs is mainly influenced by the extinction coefficient (k), spectral reflectance (ρ), thickness (L) and test wavelength (λ). When there is no phase change, the extinction coefficient (k), spectral reflectance (ρ) and test wavelength (λ) are constant values. Eq. (11) and Eq. (12) show that τ'_{solid} and τ'_{liquid} are always negatively affected by thickness. Meanwhile, τ'_{solid} and τ'_{liquid} is an exponential functions, the transmittance and thickness do not have a simple linear relationship, which is also shown in the experimental results. However, Eq. (11) is only calculated for the two-interface case, while the number of interfaces increased significantly after the PCM's solidification.

3.2.3 Transmittance in MIR for different phases and thicknesses

Fig. 5 shows the spectroscopic measurements of the "atmospheric window" (8-13 μm) by FTIR. The thicknesses of PCM samples were measured by the electronic spiral micrometer.

The spectral transmittance of liquid n-alkanes with three thicknesses is shown in Figs. 5 (a), (c) and (e). For n-Hexadecane, the average transmittance in 8-13 μm decreased from 73% to 54.5% and 34% when the thickness increased from 243 μm to 468 μm (increased 93%) and to 1072 μm (increased 341%). For n-Octadecane, the average transmittance in 8-13 μm decreased from 84.7% to 74.8% and 33% when the thickness increased from 154 μm to 293 μm (increased 90%) and to 901 μm (increased 485%). For n- Eicosane, the average transmittance in 8-13 μm decreased from 54% to 47.8% and 16% when the thickness increased from 350 μm to 529 μm (increased 51%) and to 1380 μm (increased 294%). It can therefore be seen that the change in transmittance in the 8-13 μm band was significantly affected by the thickness in the liquid state.

As presented in Figs. 5 (b), (d) and (f), the spectral transmittance of the solid n-alkanes with three thicknesses do show significant differences with the liquid state of Figs. 5 (a), (c) and (e). For n-Hexadecane, the average transmittance in 8-13 μm decreased

from 28% to 8% and 6% when the thickness increased from 318 μm to 678 μm (increased 113%) and to 1050 μm (increased 230%). For n-Octadecane, the average transmittance in 8-13 μm decreased from 42% to 27.5% and 22.3% when the thickness increased from 154 μm to 388 μm (increased 152%) and to 825 μm (increased 436%). For n-Eicosane, the average transmittance in 8-13 μm decreased from 16% to 5.5% and 0.7% when the thickness increased from 415 μm to 610 μm (increased 47%) and to 1344 μm (increased 223%). Overall, the measurements showed that the transmittance in the 8-13 μm band was also considerably affected by the thickness in the solid phase.

According to the analysis of UV-VIS-MIR, the transmittance of n-Hexadecane, n-Octadecane and n-Eicosane showed an extreme difference between the solid and liquid phase in both 0.19-1.1 μm and 8-13 μm band. However, the PCM thickness does show a much more significant effect on the transmittance of PCMs in the 8-13 μm band than the UV-VIS-NIR. The transmittance of n-Hexadecane, n-Octadecane and n-Eicosane at the thickness of 1000 μm was around 20% in the liquid phase, which means it is unable to meet the requirement of high transmittance as a radiative cooler cover. To this end, it is necessary to reduce the thickness of the PCM layer to develop SSC for radiative cooling.

3.2.4 Reliability analysis of the two-thickness inversion method

The optical constants (i.e. interfacial reflectance (ρ), extinction coefficient (k) and refractive index (n)) of various paraffin waxes in solid and liquid phases were calculated based on the above measurements and the two-thickness inversion method. The two groups of measured data for different thicknesses of PCM layers were used for the calculation, i.e. the thickness of 2 mm and 3 mm in the 0.19-1.1 μm band. Then, the optical constants data were used to calculate the transmittance of the third thickness (theoretical value) which was compared with the measured values to evaluate the reliability of the two-thickness inversion method.

Fig. 6 shows the comparison of the experimental and theoretical values in UV-VIS-NIR. It can be seen that the waveforms of the measured and inversed curves were very

close and had the same absorption peaks. In addition, the difference in average transmittance between the theoretical and measured values for liquid n-Hexadecane, n-Octadecane and n-Eicosane was respectively only 1.5%, 1.2% and 1.5% in the 0.19-1.1 μm band. For the solid phase of n-Hexadecane, n-Octadecane and n-Eicosane, the difference in average transmittance between the theoretical and experimental analysis was just 0.1%, 0.3% and 0.7%, respectively. The maximum difference between the theoretical and experimental values was 9.3% at the PCM absorption peak, possibly because the absorption has resulted in an abrupt change of optical constants.

Fig. 7 shows the comparison of the experimental and theoretical values in the 8-13 μm band. The difference in average transmittance between the theoretical and measured values for liquid n-Hexadecane, n-Octadecane and n-Eicosane was only 1.6%, 1% and 3%, respectively. For the solid phase, the difference in average transmittance between the theoretical and experimental values was 13.1%, 6.4% and 6% for n-Hexadecane, n-Octadecane and n-Eicosane, respectively. The maximum difference between the theoretical and experimental values was 13.1% for n-Hexadecane, which may be due to the increased interfaces between solid-PCM grains that resulted in Mie scattering [29, 30] or due to a PCM thickness measurement error.

According to the experimental tests, the PCM thickness measurement errors may have caused a significant difference between theoretical and experimental values for the FTIR testing. There are two main reasons for that: 1) The thickness of the PCM layer was calculated by the total thickness of KBr infrared absorption cell minus the thickness of two KBr windows. Although the measurement accuracy of the electronic spiral micrometer was as high as 1 μm, the thickness of the KBr window (3981 μm) is much larger than the PCM layer and might cause a relatively large error in measuring the PCM layer thickness. Therefore, the thicknesses at four different points were measured and used the average PCM layer thickness for the theoretical calculation. 2) The preheating and precooling temperature was 70 ºC and 0 ºC for the FTIR testing of the liquid and solid PCM samples, while the room temperature was 20 ºC. These temperature changes during the measurements might also cause thickness measurement

differences in the PCM layer. For instance, this can be indicated by the density of n-Octadecane, which is 775 kg/m^3 in the liquid state, and 814 kg/m^3 in the solid state[31].

Comparison analysis shows that the two-thickness inversion method curve has the same position of the characteristic peaks and the same curve shape as the measured results. In the UV-VIS-NIR band, the error in the two-thickness inversion method was less than 1.5%. In the 8-13 μm band, the average error of the two-thickness inversion method was no more than 3% in the liquid phase. Except for the solid phase in 8-13 μm, the inversion error was relatively low, and the obtained optical constants were quite stable and acceptable in both spectral bands.

3.2.5 Optical constants comparison of PCM in solid and liquid

The extinction coefficient (k) and reflectance (ρ) for paraffin in solid and liquid states were calculated by Eqs. (6), (8), (9) and (10), as shown in Fig. 8 In the 0.3-1.1 μm band, the extinction coefficient (k) of liquid paraffin (Fig. 8 (a)) slowly increased with increasing wavelength. The average extinction coefficient was around 3×10^{-7}. The extinction coefficient (k) for solid paraffin (Fig. 8 (b)) also increased with increasing wavelength, but the increasing rate was more obvious than in the liquid state. The extinction coefficient (k) for solid paraffin increased from 8×10^{-6} to 2.2×10^{-5}, while the average extinction coefficient was around 1.4×10^{-5}. The spectral reflectance (ρ) of liquid paraffin (Fig. 8 (c)) was stabilized below 9%, but ρ in solid (Fig. 8 (d)) was much larger and between 80% and 90%. The maximum ρ difference between the solid and liquid states was as much as 88%. The extinction coefficient (k) and spectral reflectance (ρ) of solid paraffin were much higher than in the liquid phase. The average k for the n-Hexadecane, n-Octadecane and n-Eicosane samples in the solid phase was 55, 69 and 57 times higher than the liquid, and the average ρ for n-Hexadecane, n-Octadecane and n-Eicosane samples in the solid-state was 22, 23 and 20 times higher than the liquid state.

In the “atmospheric window” of the 8-13 μm band, the average extinction coefficient (k) for n-Hexadecane, n-Octadecane and n-Eicosane samples (Figs. 8 (a) and (b)) in the

solid-state were 0.6, 0.7 and 2.9 times of the liquid, while spectral reflectance (ρ) for n-Hexadecane, n-Octadecane and n-Eicosane samples (Figs. 8 (c) and (d)) in solid was 7, 6.7 and 1.8 times of the liquid phase. In the MIR band, the difference in reflectance between the solid and liquid states was not as much as in the UV-VIS-NIR band, but the maximum difference was still about 61%. In conclusion, the reflectance and extinction coefficient of paraffin in liquid and solid phases demonstrated a significant difference, which led to paraffin having considerably different transmittance in different states and formed thermogenic spectral transmission switching effects during the phase change period.

3.2.6 Microstructure of PCM grain in solid phase

The morphology of phase change grain growth is mainly dependent on the structure of the liquid/solid interface, the external conditions, the thermal conductivity of materials, and the cooling rate [32]. The solidification process of paraffin was affected by impurities and external surfaces in this study, which generated large amounts of non-uniform nucleation [32, 33] and formed several differently shaped paraffin crystals [32, 34], see supplementary video: Solidification of n-Eicosane. Fig. 9 (a) shows a microscopic image of solid n-Eicosane which was interlaced and irregular grain boundaries between different PCM particles. Fig. 9 (b) shows the particle size distribution of the PCM grain and the PCM crystalline average particle scale was around 10 μm, which is much larger than the wavelength of UV-VIS-NIR (0.19-1.1 μm). When the particle size is close to the wavelength of the incident light (8-13 μm), the incident MIR light will be strongly scattered and result in Mie scattering [35]. Meanwhile, the scattered light intensity is asymmetrical in all directions, and the larger the particle sizes, the higher the forward scattering. Therefore, when incident light passes through the multilayer-like structure, it will undergo the Mie scattering phenomenon [29, 30], which will result in a significant reduction in the final transmittance of UV-VIS-NIR. And this reduction in the transmittance would also appear in the MIR (8-13 μm) because the average diameter of the PCM crystalline is

close to the wavelength of MIR and resulted in Mie scattering. To this end, this reduction in the transmittance of UV-VIS-NIR-MIR was reflected in the macroscopic appearance of milky white colour, as shown in Fig. 9 (c).

3.3 Transmittance properties of SSC

The n-Hexadecane, n-Octadecane and n-Eicosane were used as the PCM layer to produce three SSC samples, where the thickness of the PE film is 100 μm and the thickness of the PCM layer is around 300 μm. The transmittance in Fig. 10 showed the obvious transmittance difference between the solid and liquid phase states of PCM. Meanwhile, the transmittance curve of the SSC in the liquid state was influenced at the same time by the PCM and PE film. However, the transmittance of the SSC was mainly determined by the solid PCM because the transmittance of the solid PCM layer was much lower than the PE film. In the 0.19-1.1 μm band, the average transmittance decreased from 90% to 0.6% for n-Hexadecane, from 88% to 0.7% for n-Octadecane, and from 89% to 0.7% for n-Eicosane after solidification. In the 8-13 μm band, the average transmittance also decreased from 39.3%, 40.3% and 28.9% to 3.7%, 2.2% and 2.7% after solidification for n-Hexadecane, n-Octadecane and n-Eicosane, respectively.

The above results proved the temperature-adaptive switching properties of the SSC in liquid and solid phases.

To achieve radiative cooling, the power radiated by the emitter must be higher than the absorbed heat from the sunlight and environment[2]. The integrated SSC into a static radiative cooler would change the radiative heat transfer process between the emitter and outer space. For example, when the ambient temperature is higher than the melting points of the PCM layer, the SSC has a high transmittance and switches on radiative heat transfer between the emitter and outer space. In contrast, the radiative heat transfer would switch off when the PCM is in solid phase due to its low transmittance.

However, the average transmittance of the developed SSC was only 40% in the atmospheric window, which cannot meet the requirement of high transmission in the 8-13 μm and would affect the output power of the radiative cooler. According to sections

3.2.2 and 3.2.3, the transmittance of the PCM layer in 8-13 μm was significantly affected by the thickness of the PCM layer. According to the calculation in Eq. (1), the transmittance of the liquid PCM layer would be more than 80% when the PCM thickness is 100 μm. In addition, the transmittance of the PE film can also reach more than 90% in the 2.5-25 μm band when the thickness of the PE film is at 10 μm [36]. This means using thinner PE and PCM layers can improve the transmittance of SSC in the switch-on state. Although the SSC would possibly achieve self-temperature adaptive radiative cooling, further experimental verifications of the performance of the dynamic radiative cooling system are needed.

4 Conclusions and outlook

This study selected paraffin waxes as PCMs to develop a low-cost SSC for dynamic radiative cooling systems. Based on experimental data, the optical constants of paraffin are inverted by the two-thickness inversion method to resolve the switching principle of PCM during the phase change. The microstructure analysis of PCM crystals revealed that the PCM grain formed a multilayer-like structure, resulting in a large amount of scattering of the incident light and a decrease in transmittance. In the end, three types of PE-PCM-PE triple-layer SSC were prepared and tested. The specific findings are as follows:

1) In the 0.19-1.1 μm band, the spectral transmittance of paraffin remained below 5% in the solid phase but exceeded 90% in the liquid phase. The transmittance of paraffin only decreased by 0.7-0.8% when the thickness of the PCM layer was doubled.

2) In the 8-13 μm band, the transmittance of paraffin in the liquid phase was much higher than in the solid phase at the same thickness, and the maximum difference could reach 41.1% for n-Hexadecane at the thickness of 318 μm. However, the transmittance of paraffin was significantly affected by the thickness in the MIR band.

3) The calculation error of the two-thickness inversion method for the transmittance of paraffin was 1.5% in the 0.19-1.1 μm band. The average error was 3% in the 8-13 μm

band in the liquid phase.

4) The extinction coefficient and spectral reflectance of the solid PCM increased by 20-23 and 55-69 times respectively compared with the liquid state in UV-VIS-NIR, and this in turn caused a transmissive switch-off effect.

5) The SSC had obvious "switch-on" and "switch-off" states, but it was necessary to reduce the thickness of the PE and PCM layers to optimize the dynamic radiative cooling system.

In conclusion, the optical transmission properties of n-Hexadecane, n-Octadecane and n-Eicosane were measured, and the reliability of the two-thickness inversion method to calculate the optical constants of PCM was verified. The study successfully produced a low-cost SSC to realize the automatic temperature adaptive switching of radiative heat transfer between a radiative cooler and outer space. However, the temperature-adaptive SSC in this study still shows some limitations. For instance, the mid-infrared transmittance of SSC needs to be further increased for effective radiative cooling, which requires the use of thinner PE films and PCM layers. Furthermore, the thickness of PCM in SSC might change in the liquid phase as a result of gravity, and therefore the pretension and mechanical strength of SSC film will need to be considered. The performance of SSC in radiative cooling systems will also need further experimental evaluation.

Acknowledgements: This work was supported by the Young Scientists Fund of National Natural Science Foundation of China (NSFC) (No. 51908299); Young Innovative Talents Introduction & Cultivation Program for Colleges and Universities of Shandong Province (Granted by Department of Education of Shandong Province, Sub-Title 1: Innovative Research Team of Advanced Energy Equipment, Sub-Title 2: Innovative Research Team of High Performance Integrated Device); Qing Chuang science and technology plan of colleges and universities in Shandong Province (No. 2019KJB009); Taishan Scholars Foundation of Shandong Province (No. tsqn201812087); Jinan Scientific Research Leader Studio (No. 2021GXRC083). We also thank Mr. Zhen Xu for his help with experimental measurements.

References

[1] Ahmad EZ, Sopian K, Jarimi H, Fazlizan A, Elbreki A, Abd Hamid AS, et al. Recent advances in passive cooling methods for photovoltaic performance enhancement. International Journal of Electrical and Computer Engineering (IJECE). 2021;11. https://doi.org/10.11591/ijece.v11i1.pp146-154.

[2] Raman AP, Anoma MA, Zhu L, Rephaeli E, Fan S. Passive radiative cooling below ambient air temperature under direct sunlight. Nature. 2014;515:540-4. https://doi.org/10.1038/nature13883.

[3] Kou J-l, Jurado Z, Chen Z, Fan S, Minnich AJ. Daytime Radiative Cooling Using Near-Black Infrared Emitters. ACS Photonics. 2017;4:626-30. https://doi.org/10.1021/acsphotonics.6b00991.

[4] Chae D, Kim M, Jung P-H, Son S, Seo J, Liu Y, et al. Spectrally Selective Inorganic-Based Multilayer Emitter for Daytime Radiative Cooling. ACS applied materials & interfaces. 2020;12:8073-81. https://doi.org/10.1021/acsami.9b16742.

[5] Ma H, Yao K, Dou S, Xiao M, Dai M, Wang L, et al. Multilayered SiO2/Si3N4 photonic emitter to achieve high-performance all-day radiative cooling. Solar Energy Materials and Solar Cells. 2020;212. https://doi.org/10.1016/j.solmat.2020.110584.

[6] Zhao D, Aili A, Zhai Y, Lu J, Kidd D, Tan G, et al. Subambient Cooling of Water: Toward Real-World Applications of Daytime Radiative Cooling. Joule. 2019;3:111-23. https://doi.org/https://doi.org/10.1016/j.joule.2018.10.006.

[7] Tsilingiris PT. Comparative evaluation of the infrared transmission of polymer films. Energy Conversion and Management. 2003;44:2839-56. https://doi.org/10.1016/s0196-8904(03)00066-9.

[8] Leroy A, Bhatia B, Kelsall CC, Castillejo-Cuberos A, H. MDC, Zhao L, et al. High-performance subambient radiative cooling enabled by optically selective and thermally insulating polyethylene aerogel. SCIENCE ADVANCES. 2019.

[9] Mehling H, Leys J, Glorieux C, Thoen J. Potential new reference materials for caloric measurements on PCM. SN Applied Sciences. 2021;3. https://doi.org/10.1007/s42452-020-03929-y.

[10] Kana Kana JB, Vignaud G, Gibaud A, Maaza M. Thermally driven sign switch of static dielectric constant of VO2 thin film. Optical Materials. 2016;54:165-9. https://doi.org/https://doi.org/10.1016/j.optmat.2016.02.032.

[11] Wang H, Yang Y, Wang L. Switchable wavelength-selective and diffuse metamaterial absorber/emitter with a phase transition spacer layer. Applied Physics Letters. 2014;105. https://doi.org/10.1063/1.4893616.

[12] Ono M, Chen K, Li W, Fan S. Self-adaptive radiative cooling based on phase change materials. Opt Express. 2018;26:A777-A87. https://doi.org/10.1364/OE.26.00A777.

[13] Wu SR, Lai KL, Wang CM. Passive temperature control based on a phase change metasurface. Sci Rep. 2018;8:7684. https://doi.org/10.1038/s41598-018-26150-9.

[14] Long L, Taylor S, Ying X, Wang L. Thermally-switchable spectrally-selective infrared metamaterial absorber/emitter by tuning magnetic polariton with a phase-change VO2 layer. Materials Today Energy. 2019;13:214-20.

https://doi.org/https://doi.org/10.1016/j.mtener.2019.05.017.
[15] Abedini Dereshgi S, Larciprete MC, Centini M, Murthy AA, Tang K, Wu J, et al. Tuning of Optical Phonons in alpha-MoO3-VO2 Multilayers. ACS applied materials & interfaces. 2021. https://doi.org/10.1021/acsami.1c12320.
[16] Zhao H, Zhan Y, Dou S, Wang L, Li Y, Li X. Passive radiative temperature regulator: Principles and absorption-emission manipulation. Solar Energy Materials and Solar Cells. 2021;229. https://doi.org/10.1016/j.solmat.2021.111143.
[17] Xu X, Gu J, Zhao H, Zhang X, Dou S, Li Y, et al. Passive and Dynamic Phase-Change-Based Radiative Cooling in Outdoor Weather. ACS Appl Mater Interfaces. 2022. https://doi.org/10.1021/acsami.1c23401.
[18] Bhattacharya RN. CIGS-based solar cells prepared from electrodeposited stacked Cu/In/Ga layers. Solar Energy Materials and Solar Cells. 2013;113:96-9. https://doi.org/10.1016/j.solmat.2013.01.028.
[19] Merck. Octadecane. Merck KGaA, Darmstadt, Germany and/or its affiliates: https://www.sigmaaldrich.cn/CN/en/search/octadecane?focus=products&page=1&perpage=30&sort=relevance&term=octadecane&type=product.
[20] Merck. Vanadium dioxide. Merck KGaA, Darmstadt, Germany and/or its affiliates: https://www.sigmaaldrich.cn/CN/zh/search/vanadium-dioxide?focus=products&page=1&perpage=30&sort=relevance&term=vanadium%20dioxide&type=product.
[21] Zhao D, Zhang G, Zhang X, Li D. Optical properties of paraffin at temperature range from 40 to 80 °C. Optik. 2018;157:184-9. https://doi.org/10.1016/j.ijleo.2017.11.093.
[22] Su W, Cai P, Kang R, Wang L, Kokogiannakis G, Chen J, et al. Development of temperature-responsive transmission switch film (TRTSF) using phase change material for self-adaptive radiative cooling. Applied Energy. 2022;322. https://doi.org/10.1016/j.apenergy.2022.119457.
[23] Zheng Y. Research on Photo-thermal Performance of PCM-filled Glazing Roof in severe cold area [D]: Northeast Petroleum University; 2017.
[24] Tuntomo A, Tien CL, Park SH. Optical Constants of Liquid Hydrocarbon Fuels. Combustion Science and Technology. 1992;84:133-40. https://doi.org/10.1080/00102209208951849.
[25] Turner, W. R. Normal Alkanes. Industrial & Engineering Chemistry Product Research and Development. 1971;10:238-60.
[26] 50785-2012 GT. Evaluation standard for indoor thermal environment in civil buildings. Standardization Administration of China Beijing; 2012.
[27] Cabeza LF, Castell A, Barreneche C, de Gracia A, Fernández AI. Materials used as PCM in thermal energy storage in buildings: A review. Renewable and Sustainable Energy Reviews. 2011;15:1675-95. https://doi.org/10.1016/j.rser.2010.11.018.
[28] Genovese A, Amarasinghe G, Glewis M, Mainwaring D, Shanks RA. Crystallisation, melting, recrystallisation and polymorphism of n-eicosane for application as a phase change material. Thermochimica Acta. 2006;443:235-44. https://doi.org/10.1016/j.tca.2006.02.008.
[29] Apostoleris HN, Chiesa M, Stefancich M. Improved transparency switching in paraffin–PDMS composites. Journal of Materials Chemistry C. 2015;3:1371-7. https://doi.org/10.1039/c4tc02546f.
[30] Hahn DW. Light scattering theory. Department of Mechanical and Aerospace Engineering, University of Florida. 2009.

[31] Su W, Darkwa J, Kokogiannakis G. Review of solid–liquid phase change materials and their encapsulation technologies. Renewable and Sustainable Energy Reviews. 2015;48:373-91. https://doi.org/10.1016/j.rser.2015.04.044.
[32] Kim D-e, Park S, Choi YH, Han SH, Kim S-H. Crystallization and Melting of Thermoresponsive Colloids Confined in Microcapsules. Chemistry of Materials. 2022. https://doi.org/10.1021/acs.chemmater.2c00448.
[33] Zhang H. FABRICATION AND PERFORMANCE OF COMPOSITE PHASE CHANGE MATERIAL THROUGH SELF-ASSEMBLY TECHNOLOGY: Beijing University of Chemical Technology; 2010.
[34] Akyurt M, Zaki G, Habeebullah B. Freezing phenomena in ice–water systems. Energy Conversion & Management. 2002;43:1773-89.
[35] Mie G. Beiträge zur Optik trüber Medien, speziell kolloidaler Metallösungen. Annalen der physik. 1908;330:377-445.
[36] Zhang J, Yuan J, Liu J, Zhou Z, Sui J, Xing J, et al. Cover shields for sub-ambient radiative cooling: A literature review. Renewable and Sustainable Energy Reviews. 2021;143. https://doi.org/10.1016/j.rser.2021.110959.

Table 1 Raw materials

Materials	Molecular formula	Density (g/mL)	Melting point (ºC)	Producer
Polyethylene	-[-CH2-CH2-]n-	0.91	85-110	Shenzhen Zhenhua Adhesive Products Co., Ltd.
n-Hexadecane	C16H34	0.773	18	Shanghai Macklin Biochemical Co., Ltd
n-Octadecane	C18H38	0.777	26-29	Shanghai Macklin Biochemical Co., Ltd
n-Eicosane	C20H42	0.788	35-37	Shanghai Macklin Biochemical Co., Ltd

Table 2 Equipment list

Equipment Name	Application	Company & Specification
DSC	Testing latent heat and melting temperature of PCMs	Instruments Waters, TA25
UV-VIS spectrum spectrometer	Spectral properties testing of n-alkanes in the band 0.19-1.1 μm	Shanghai Metash Instruments, UV-8000
FTIR spectroscopy	Spectral properties testing of n-alkanes in the band 8-13 μm	BRUKER (Germany), ALPHA I
Semiconductor heating and cooling module	Preheating and precooling PCM/SSC samples	Jiangsu Xinghe Electronic Technology, XH-W1504
K-type thermocouple	Temperature monitoring of PCM/SSC samples	UNI-Trend Technology (China), TUT320D
Heating sealer	Sealing SSC samples	Xiamen Vectech Electronic Co., Ltd., BV106

Table 3 Phase change properties of PCMs

DSC testing process	PCM type	Onset temperature(ºC)	Peak temperature(ºC)	End temperature(ºC)	Latent enthalpies(J/g)
Melting	n-Hexadecane	16.2	17.9	19.2	220.5
	n-Octadecane	26.1	27.4	28.7	243.6
	n-Eicosane	35.0	36.0	37.7	248.0
Solidification	n-Hexadecane	14.4	14.7	13.1	221.4
	n-Octadecane	25.3	25.4	23.9	243.3
	n-Eicosane	34.6	33.8	32.3	248.3

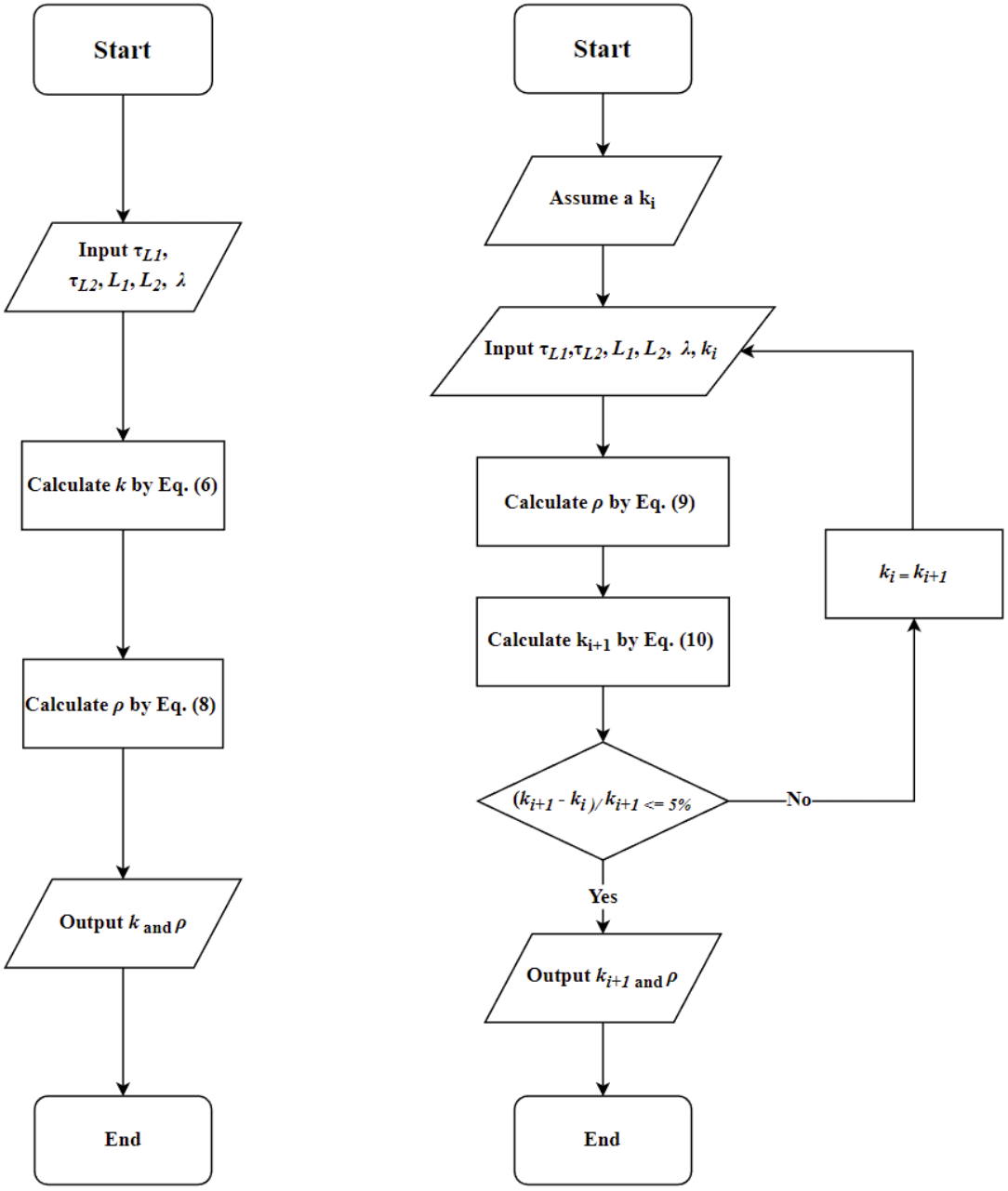

Figure 1 Matlab calculation flowchart

(Fig. 1 (a) the calculation for liquid PCM; Fig. 1 (b) the calculation for solid PCM)

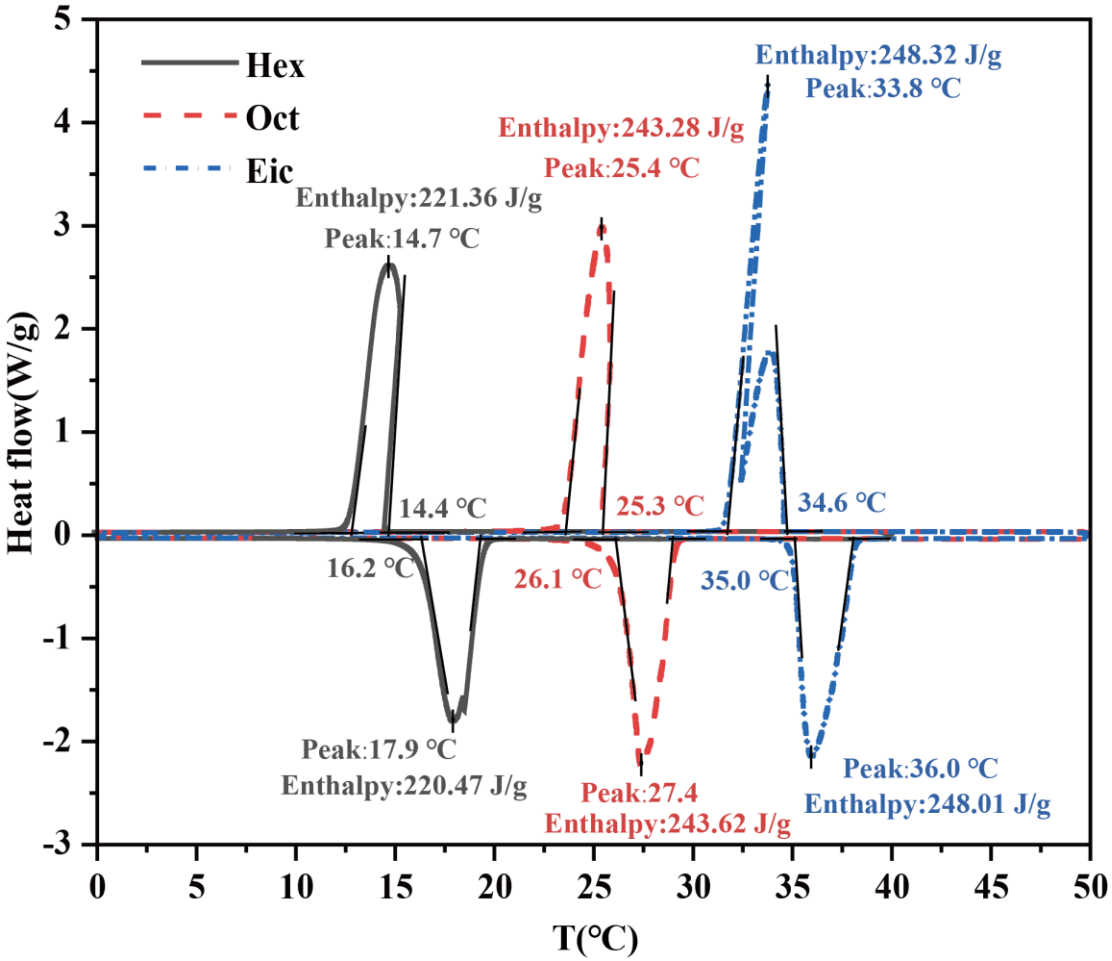

Figure 2. Melting and solidification profiles of PCM samples

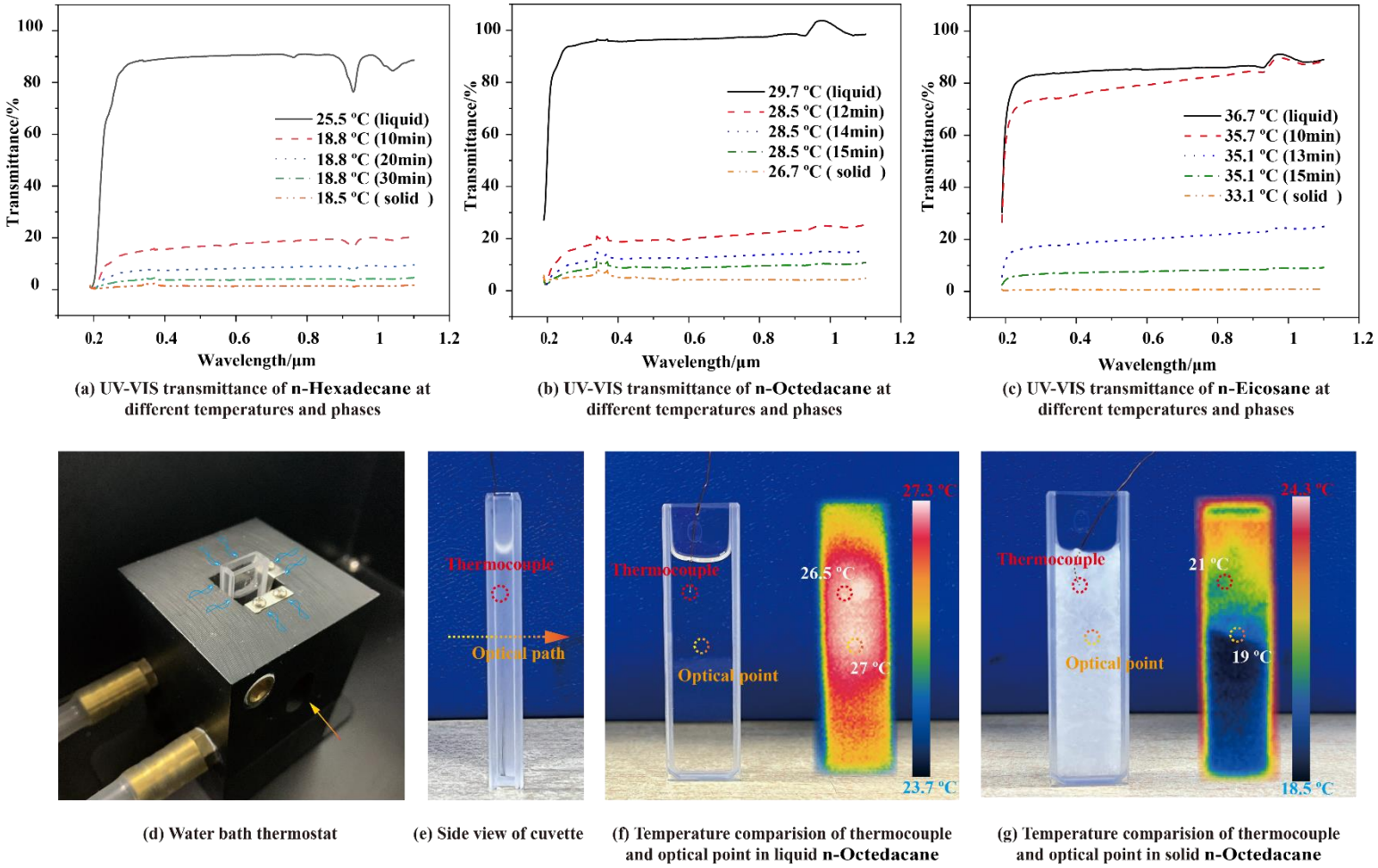

(a) UV-VIS transmittance of **n-Hexadecane** at different temperatures and phases

(b) UV-VIS transmittance of **n-Octedacane** at different temperatures and phases

(c) UV-VIS transmittance of **n-Eicosane** at different temperatures and phases

(d) Water bath thermostat

(e) Side view of cuvette

(f) Temperature comparision of thermocouple and optical point in liquid **n-Octedacane**

(g) Temperature comparision of thermocouple and optical point in solid **n-Octedacane**

Figure 3. UV-VIS transmittance of paraffin at different temperatures and phases

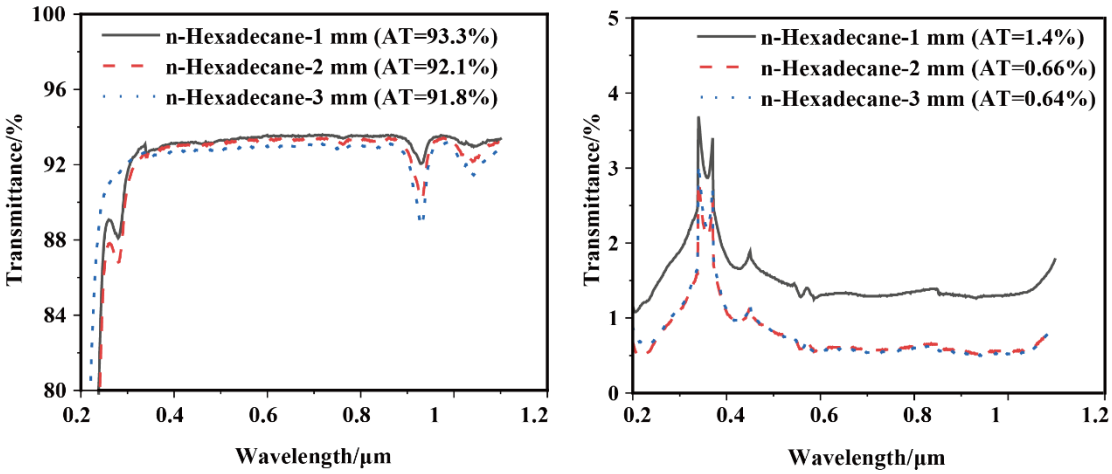

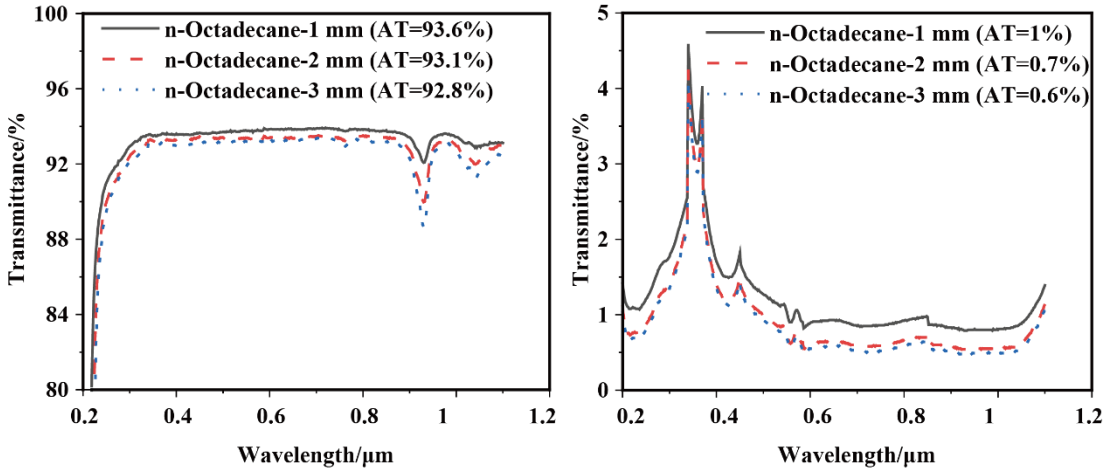

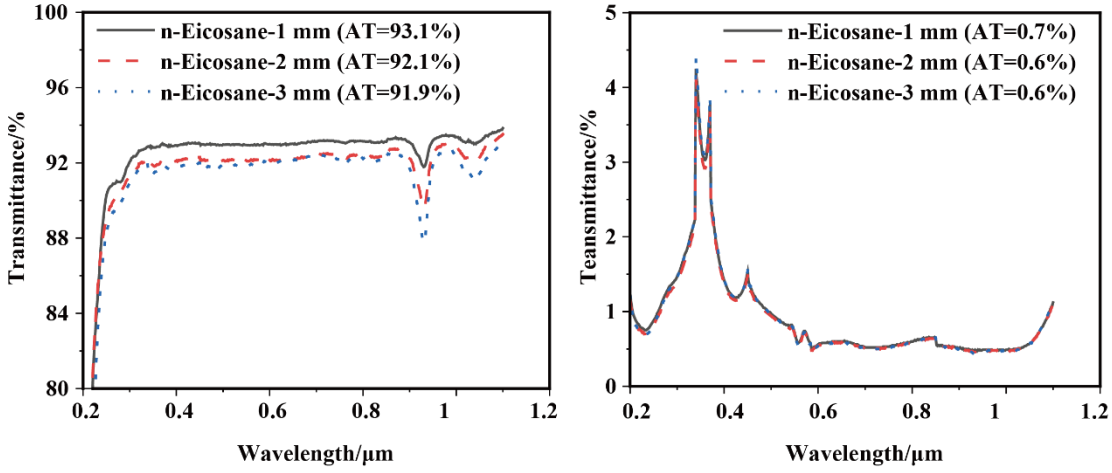

Figure 4. UV-VIS Transmittance of paraffin at different thicknesses and phase

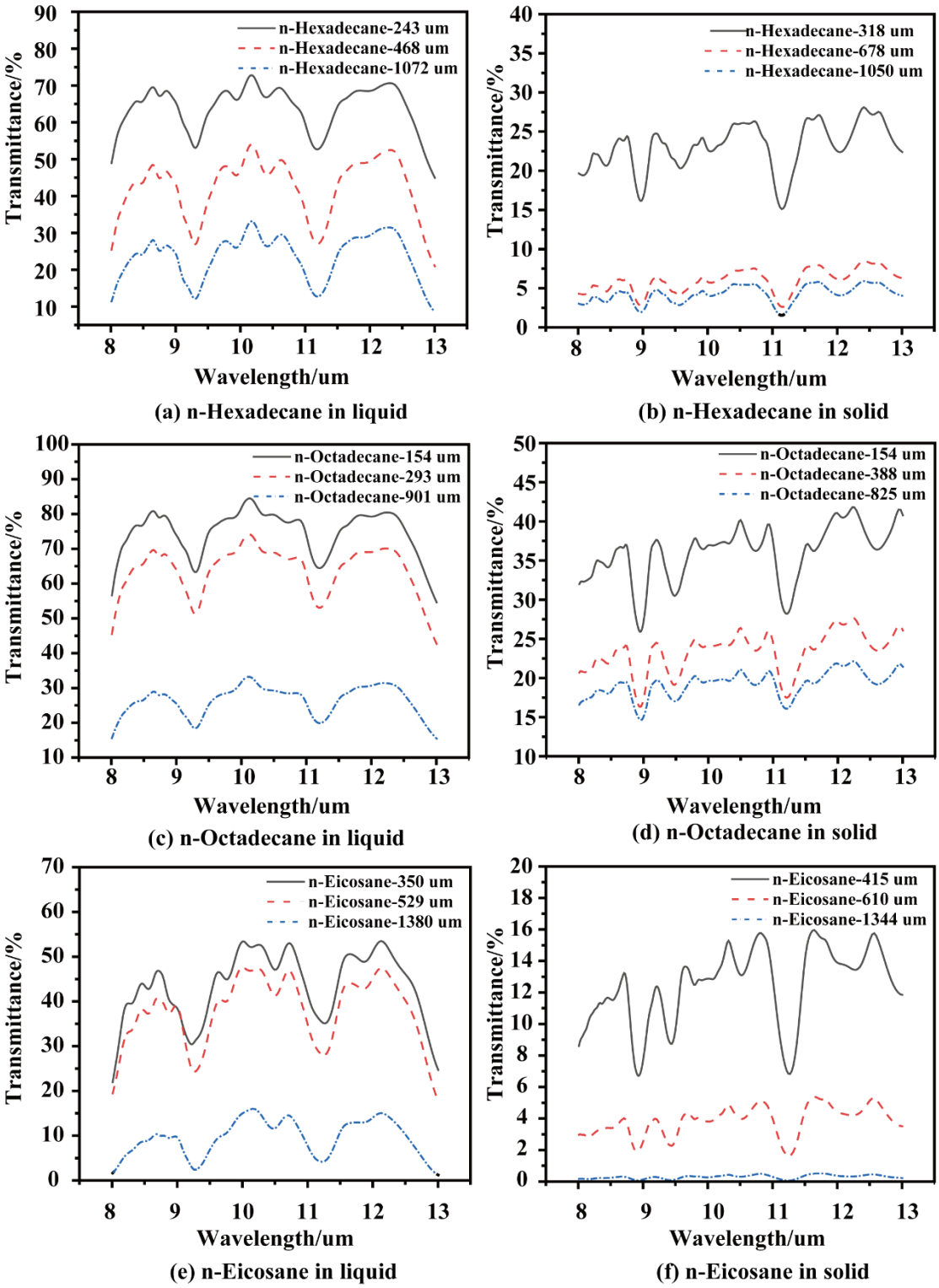

Figure 5. Transmittance in 8-13 μm band of PCMs in solid and liquid

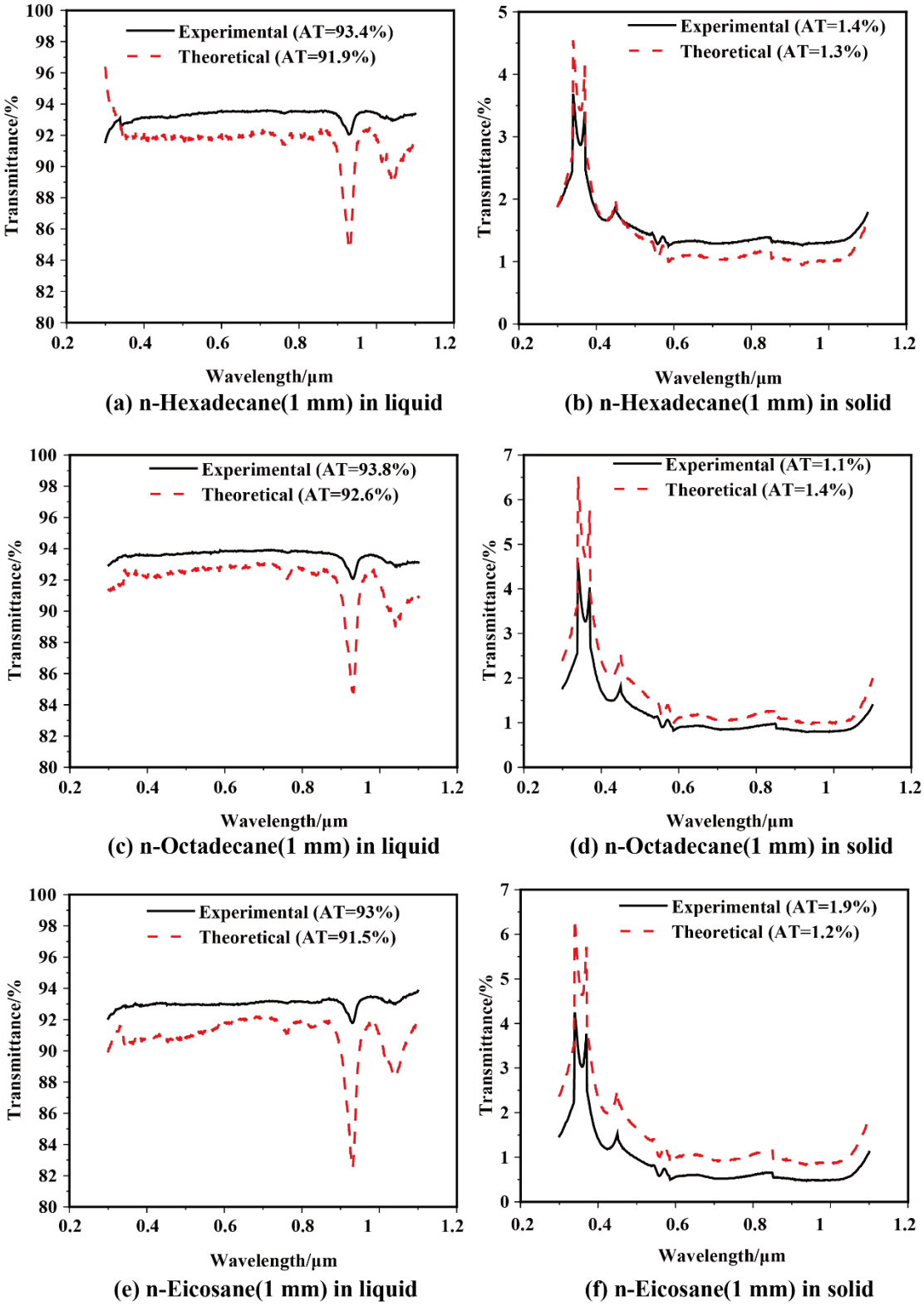

Figure 6. Experimental and theoretical profiles of UV-VIS transmittance of paraffin

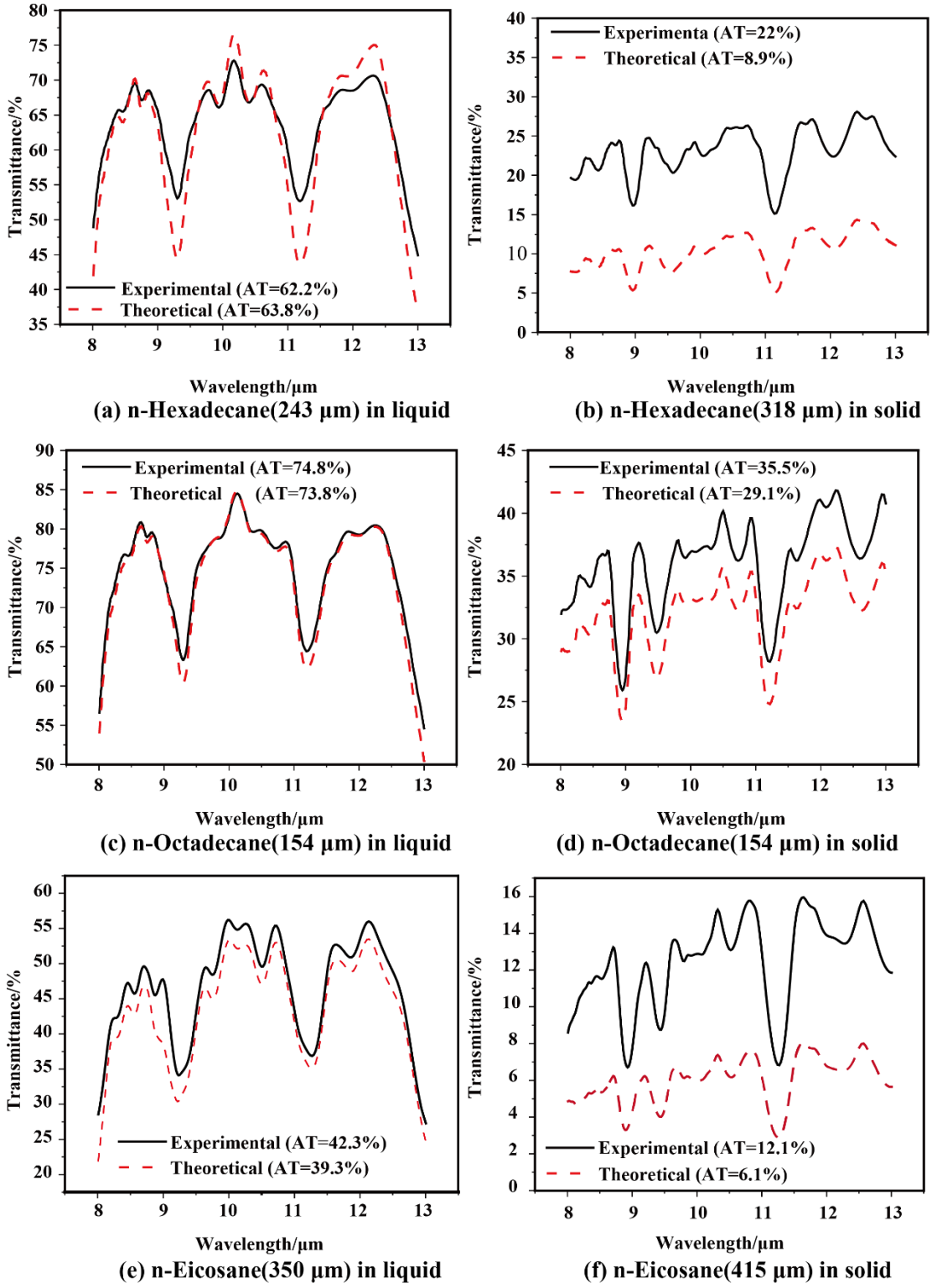

Figure 7. Experimental and theoretical transmittance of paraffin in 8-13 μm

.

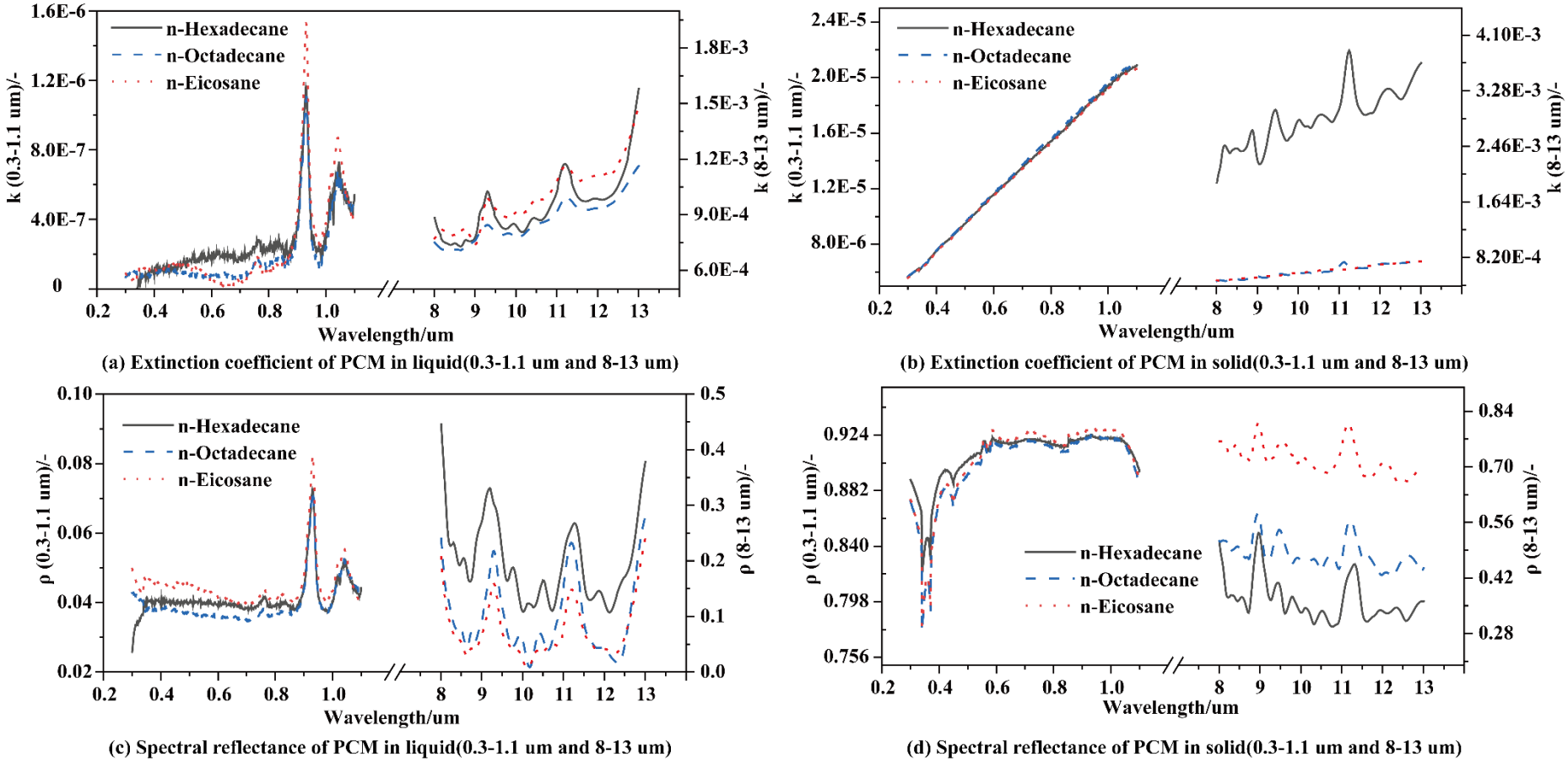

(a) Extinction coefficient of PCM in liquid(0.3-1.1 um and 8-13 um)

(b) Extinction coefficient of PCM in solid(0.3-1.1 um and 8-13 um)

(c) Spectral reflectance of PCM in liquid(0.3-1.1 um and 8-13 um)

(d) Spectral reflectance of PCM in solid(0.3-1.1 um and 8-13 um)

Figure 8. Optical constants of PCMs in liquid and solid phases

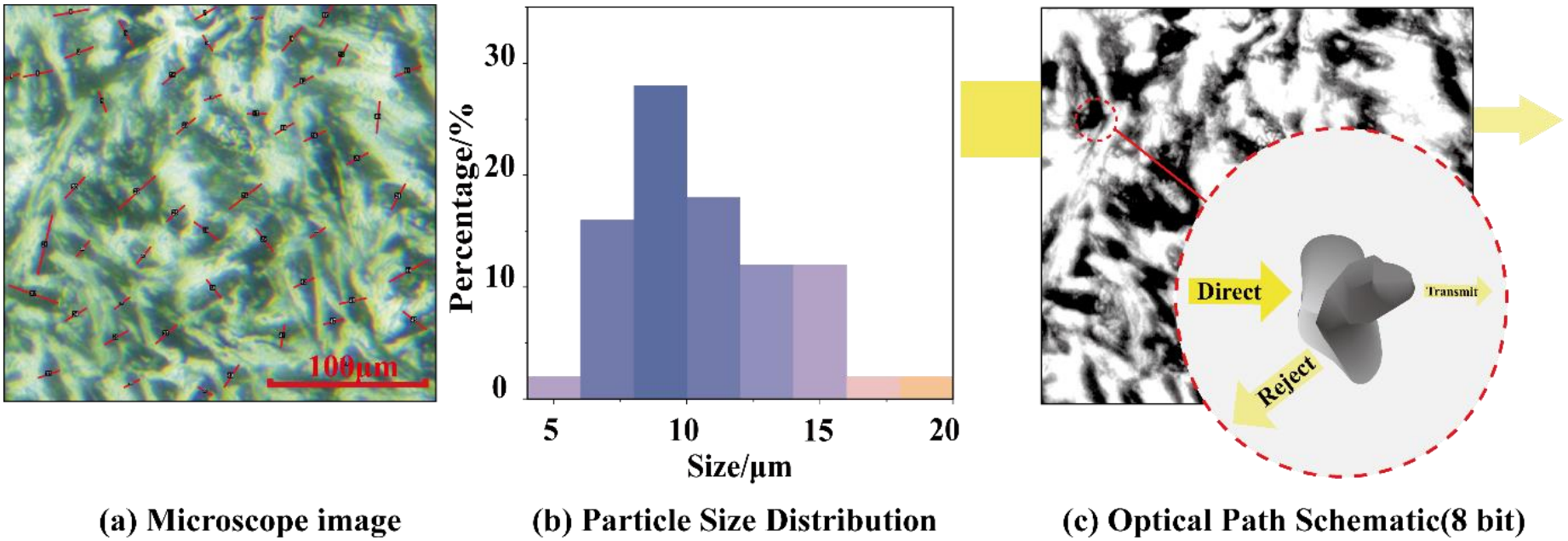

Figure 9. Microstructural analysis of solid-state n-Eicosane

（Fig. 9 (a) the microscope image of solid n-Eicosane; Fig. 9 (b) the particle size distribution of solid n-Eicosane; Fig. 9 (c) the schematic diagram of the optical path through solid n-Eicosane）

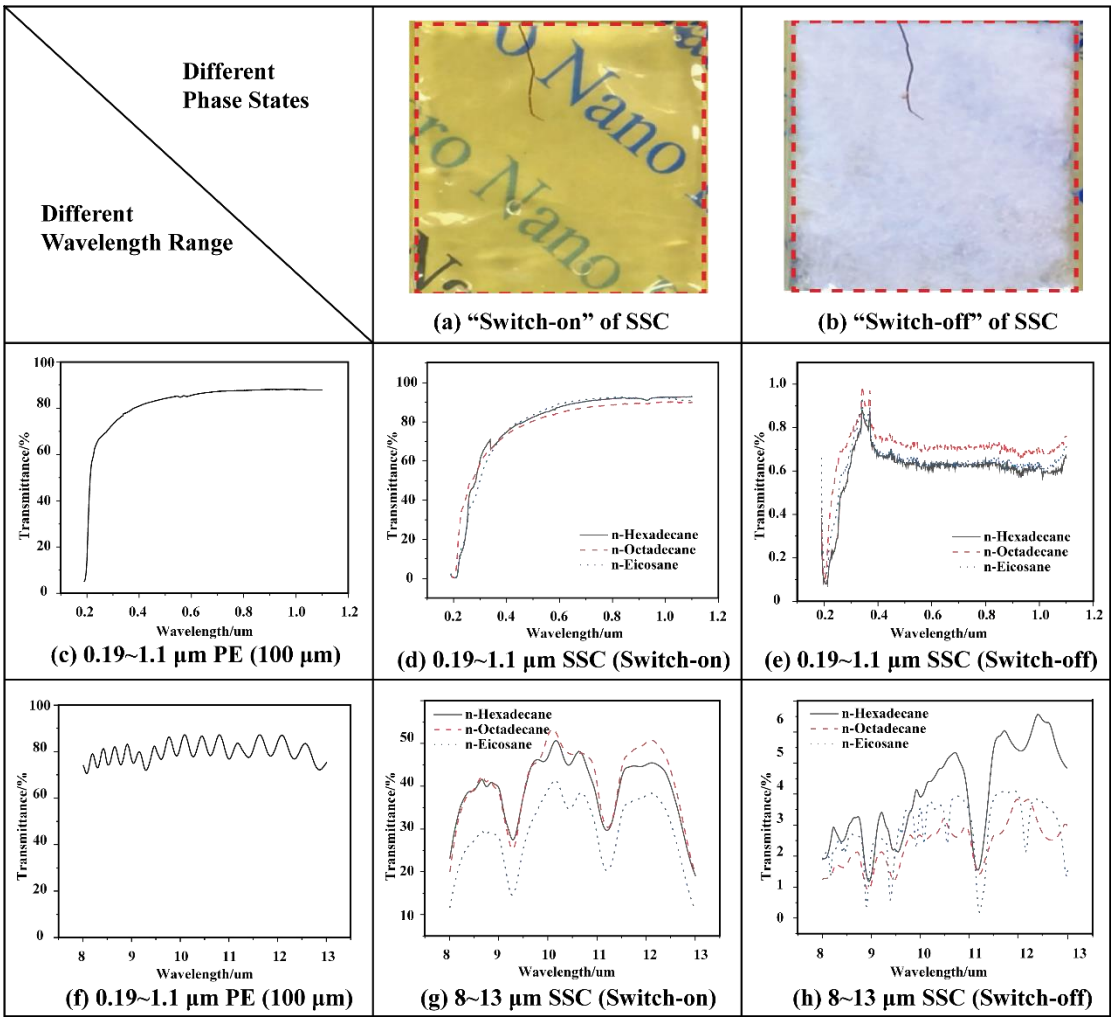

Figure 10. The transmittance property of SSC under "switch-on" and "swich-off" (Figs. 10 (a) and (b) show the photos of the SSC during "switch-on" and "swich-off" states; Figs. 10 (c) and (f) show the transmittance of the single-layer PE film in 0.19-1.1 μm and 8-13 μm; Figs. 10 (d) and (e) show the transmittance of SSC in the 0.19-1.1 μm band at "switch-on" and "swich-off" states; Figs. 10 (g) and (h) show the transmittance of SSC in the 8-13 μm band at "switch-on" and "swich-off" states)